Article type: Research article

Received Dec. 24, 2020 Accepted Jan. 10, 2021

Edited by: Zhizhong Gong, China Agricultural University, China

A histone H3K27me3 reader cooperates with a family of PHD finger-containing proteins to regulate flowering time in *Arabidopsis*

Feng Qian[1], Qiu-Yuan Zhao[1], Tie-Nan Zhang[1], Yu-Lu Li[1], Yin-Na Su[1], Lin Li[1], Jian-Hua Sui[1,2], She Chen[1,2] and Xin-Jian He[1,2*]

[1] National Institute of Biological Sciences, Beijing 102206, China

[2] Tsinghua Institute of Multidisciplinary Biomedical Research, Tsinghua University, Beijing 100084, China

Keywords: BAH, development, flowering, histone, H3K27me3, PHD, transcriptional repression

Running title: An H3K27me3 reader regulates flowering time

*Correspondence: Xin-Jian He (hexinjian@nibs.ac.cn)

ABSTRACT

Trimethylated histone H3 lysine 27 (H3K27me3) is a repressive histone marker that regulates a variety of developmental processes, including those that determine flowering time. However, relatively little is known about the mechanism of how H3K27me3 is recognized to regulate transcription. Here, we identified BAH domain-containing transcriptional regulator 1 (BDT1) as an H3K27me3 reader. BDT1 is responsible for preventing flowering by suppressing the expression of flowering genes. Mutation of the H3K27me3 recognition sites in the BAH domain disrupted the binding of BDT1 to H3K27me3, leading to de-repression of H3K27me3-enriched flowering genes and an early-flowering phenotype. We also found that BDT1 interacts with a family of PHD finger-containing proteins, which we named PHD1-6, and with CPL2, a Pol II carboxyl terminal domain (CTD) phosphatase responsible for transcriptional repression. Pull-down assays showed that the PHD finger-containing proteins can enhance the binding of BDT1 to the H3K27me3 peptide. Mutations in all of the *PHD* genes caused increased expression of flowering genes and an early-flowering phenotype. This study suggests that the binding of BDT1 to the H3K27me3 peptide, which is enhanced by PHD proteins, is critical for preventing early flowering.

INTRODUCTION

Methylation of histone lysine is essential for the epigenetic regulation of gene expression in multicellular organisms, including plants. The methylation states are dynamically regulated by histone methyltransferases and histone demethylases in response to intrinsic or extrinsic cues (Xiao et al., 2016). The methylation markers are specifically recognized by the 'reader' proteins and then translated into biological function (Campos and Reinberg, 2009; Liu et al., 2010). Histone lysine residues can be mono-, di-, or tri-methylated. In *Arabidopsis thaliana*, histone

lysine methylation occurs mainly at H3K4, H3K9, H3K27, and H3K36 (Liu et al., 2010; Xiao et al., 2016). H3K27 methylation is a repressive epigenetic marker that is deposited by the conserved Polycomb Repressive Complex 2 (PRC2) in eukaryotes. In *Arabidopsis*, CURLY LEAF (CLF), SWINGER (SWN), and MEDEA (MEA), are histone methyltransferases that are responsible for the tri-methylation of H3K27 (Kohler et al., 2003a, 2003b; Chanvivattana et al., 2004). Depletion of *CLF* and *SWN* causes loss of H3K27me3 markers and leads to pleiotropic developmental defects (Lafos et al., 2011; Zhou et al., 2017); MEA is mainly required for seed development (Kohler et al., 2003a; Kohler et al., 2003b). H3K27me3 is extensively distributed in the *Arabidopsis* genome, and thousands of genes are modified with H3K27me3 (Zhang et al., 2007b). It is therefore necessary to investigate the mechanism underlying the recognition of H3K27me3 in order to understand the biological function of the histone modification.

In metazoans, the H3K27me3 markers recruit Polycomb Repressive Complex 1 (PRC1), which contributes to transcriptional repression through its E3 ubiquitin ligase activity on histone H2A (Cao et al., 2005; Piunti and Shilatifard, 2016). Plants lack several core PRC1 components, however, and the remaining PRC1 components differ considerably from their homologs in animals (Bratzel et al., 2010; Yang et al., 2013; Chen et al., 2016). Thus, despite the recognition of H3K27me3 by PRC1 in animals, the mechanism seems not to be conserved in plants. In *Arabidopsis*, LIKE HETEROCHROMATIN PROTEIN 1 (LHP1) recognizes H3K27me3 and is required for H3K27me3 maintenance and transcriptional repression by associating with PRC2 components and PWWP domain-containing proteins (Turck et al., 2007; Zhang et al., 2007a; Derkacheva et al., 2013; Zhou et al., 2018).

The Bromo Adjacent Homology (BAH) domain is commonly present in chromatin-associated proteins and is responsible for protein–protein interactions (Chambers et al., 2013; Yang and Xu, 2013). Several plant BAH domain-containing proteins have been reported to recognize histone markers. The *Arabidopsis* ORC1b, which harbors a BAH-PHD cassette at its N-terminus, is reported to bind unmodified H3 (Li et al., 2016). CHROMOMETHYLASE3 (CMT3), a plant-specific methyltransferase responsible for CHG methylation, contains a BAH domain that is responsible for recognizing H3K9me2 (Du et al., 2012). Two BAH domain-containing proteins, EARLY BOLTING IN SHORT DAYS (EBS) and SHORT LIFE (SHL), bind to H3K27me3 through their BAH domains and thereby suppress the transcription of flowering genes (Qian et al., 2018; Yang et al., 2018). The plant homeodomain (PHD) zinc finger is characterized by a conserved Cys4-His-Cys3 (C4HC3) motif and is usually found in nuclear proteins involved in chromatin-associated transcriptional regulation (Schindler et al., 1993; Aasland et al., 1995; Musselman and Kutateladze, 2011). Biochemical and structural analyses have shown that several PHD fingers can bind to either modified or unmodified histones (Li and Li, 2012; Zhao et al., 2018). Interestingly, the BAH domain-containing proteins EBS and SHL also contain a PHD domain; the PHD domain can cooperate with the BAH domain to bind bivalent histone markers of H3K27me3 and H3K4me3 (Qian et al., 2018; Yang et al., 2018). It remains to be determined, however, whether and how the BAH domain and the PHD finger cooperate when they are present in different proteins.

The proper timing of flowering is precisely regulated in response to endogenous or environmental cues in *Arabidopsis*. Hundreds of genes are involved in the control of flowering time and compose several flowering pathways (Amasino, 2010; Cho et al., 2017). Among those genes, *FLOWERING LOCUS T* (*FT*)

encodes a floral integrator that is produced in leaf tissue and transported to the shoot apical meristem to promote flowering (Corbesier et al., 2007; Jaeger and Wigge, 2007). SUPPRESSOR OF OVEREXPRESSION OF CONSTANTS1 (SOC1), a MADS box transcription factor, is reported to promote flowering together with FT (Jung et al., 2012). The expression of *SOC1* can be positively regulated by FT and negatively regulated by the flowering repressor FLOWERING LOCUS C (FLC) (Yoo et al., 2005; Searle et al., 2006). Another MADS box transcription factor, AGAMOUS-LIKE 6 (AGL6), negatively regulates *FLC* and positively regulates *FT* (Yoo et al., 2011). *FRUITFULL* (*FUL*) also encodes a MADS box transcription factor, which controls the floral meristem identification in response to floral inductive signals (Ferrandiz et al., 2000), and also controls the fates of the inflorescence meristem (Balanza et al., 2018; Balanza et al., 2019). The accumulation of *FUL* in the floral meristem is promoted by FT and contributes to the transition to flowering (Teper-Bamnolker and Samach, 2005).

Previous studies indicated that H3K27me3 is enriched in a number of flowering genes, including *FT* and *SOC1* (Hou et al., 2014; Shafiq et al., 2014; Jing et al., 2019). However, relatively little is known about how the H3K27me3 marker is recognized to regulate the transcription of these genes. Here, we identified an H3K27me3 reader protein, BAH domain-containing transcriptional regulator 1 (BDT1), through affinity purification using the H3K27me3 peptide. We used biochemical assays and comparative modeling to reveal the BDT1 binding properties on H3K27me3. BDT1 specifically binds to the H3K27me3-enriched flowering genes *FT*, *SOC1*, *AGL6*, and *FUL*, and thereby prevents flowering by suppressing the transcription of these genes. We also found that a family of PHD finger-containing proteins interact with BDT1 and enhance the binding of BDT1 to the H3K27me3 peptide. Like BDT1, these PHD finger-containing proteins can

also prevent flowering by suppressing the expression of flowering genes. This study increases our understanding of how H3K27me3 is translated into flowering repression in plants.

RESULTS

BDT1 was co-purified with H3K27me3 peptide

To identify new histone H3K27me3 readers, we incubated synthesized biotinylated H3K27me3 (21-44 aa) peptide with nuclear extracts of the inflorescence tissue from wild type (WT) *Arabidopsis* (Col-0); H3 (21-44 aa) peptide was used as a negative control. The peptides and their captured proteins were affinity purified with streptavidin beads and were analyzed with mass spectrometry (MS). Three BAH domain-containing proteins, BDT1 (AT4G11560/AIPP3) (Han et al., 2016), EBS, and SHL, were co-purified with the H3K27me3 peptide but not with the unmodified H3 peptide (Figure 1A). The BAH domains of EBS and SHL were previously reported as H3K27me3 readers (Li et al., 2018; Qian et al., 2018; Yang et al., 2018). Several BAH domain-containing proteins were also found to recognize H3K27me3 markers in mammals (Zhao et al., 2016; Fan et al., 2020). We therefore suspected that BDT1 was a potential H3K27me3 reader. The association of BDT1 with the H3K27me3 peptide was further confirmed by a peptide affinity purification assay using the inflorescence tissue of *BDT1-FLAG* transgenic plants. Consistent with the MS results, BDT1-FLAG protein was present in the H3K27me3 peptide pull-down products but not in the H3 peptide pull-down products (Figure 1B). These results suggest that BDT1 specifically recognizes H3K27me3.

When we aligned the BAH domain of BDT1 (BDT1-BAH) with the BAH domains of EBS (EBS-BAH) and SHL (SHL-BAH), we found that BDT1-BAH

shows a high degree of homology with both EBS-BAH and SHL-BAH (Figure S1A). In particular, the residues composing the canonical aromatic cage in EBS (Tyr49, Trp70, and Tyr72) and SHL (Tyr41, Trp63, and Tyr65) are conserved in BDT1 (Tyr149, Trp170, and Tyr172) (Figure S1A). In addition, the Tyr149, Trp170, and Tyr172 residues of BDT1-BAH are also conserved in species of both angiosperms and gymnosperms (Figure S1B). A comparative modeling was then performed for BDT1-BAH using the published structure of EBS-BAH (PDB ID: 5Z8L) as a template (Yang et al., 2018). The modeled structure revealed that the BDT1-BAH forms three β-sheet conformations, which is similar to EBS-BAH (Figure 1C). The H3K27me3 peptide was bound within a surface cleft on the BDT1-BAH domain and formed a stable conformation (Figure 1C, D). The BAH was predicted to have a typical aromatic cage composed of Tyr149, Trp170, and Tyr172, which was corroborated by our sequence analysis (Figure 1C, E). The modeled structure also revealed several hydrogen bonds between the BAH domain and the H3 peptide. For instance, the side chains of His198 and Asp200 form one and three hydrogen bonds with H3S28, respectively (Figure 1C). The His198 and Asp200 residues are also conserved among BDT1, EBS, and SHL (Figure S1A). These interactions are considered to fix the conformation of the His imidazole ring in order to anchor the prolyl ring of H3P30, a ring that contributes to a specific recognition of H3K27me3 in EBS-BAH from *Arabidopsis* and SHL-BAH from *Populus trichocarpa* (Qian et al., 2018; Yang et al., 2018). In addition, H3R26 forms three hydrogen bonds with the side chain of Glu142, and H3K23 forms hydrogen bonds with both Glu205 and Val207 (Figure 1C). The hydrogen bonds may contribute to the stable anchoring of the H3K27me3 peptide. These results indicate that the structure of BDT1-BAH is similar to that of EBS-BAH, and suggest that the aromatic cage composed of Tyr149, Trp170, and Tyr172 is important in tri-methylated H3K27 recognition.

BDT1 specifically recognizes H3K27me3 *in vitro*

To test the binding ability of BDT1 with H3K27me3 *in vitro*, we performed peptide pull-down assays using recombinant GST-tag and His-tag full-length BDT1 proteins. We observed that compared with unmethylated H3 peptide, tri- and di-methylated H3K27 peptides had strong binding abilities for BDT1, but that mono-methylated H3K27 peptide had only a weak binding ability for BDT1 (Figures 2A, 2B, S2A, S2B). To verify the function of the aromatic cage of BDT1 in the binding of BDT1 to the H3K27me3 peptide, we used two forms of mutated recombinant BDT1 proteins in peptide pull-down assays. Trp170 to Leu and Tyr172 to Ala mutations (termed WY-m) in BDT1 disrupted the interaction between BDT1 and all methylated H3K27 peptides, and a single mutation of Trp170 to Ala (termed W-m) was sufficient to disrupt the interaction (Figures 2A, 2B, S2A, S2B). We next used a truncated recombinant GST-tagged BDT1 protein (95-273 aa) that contained the BAH domain in peptide pull-down assays; the results were similar to those obtained with full-length BDT1 proteins (Figure S2C). These results indicate that the BAH domain of BDT1, including its aromatic cage composed of Tyr149, Trp170, and Tyr172, is essential for the binding of BDT1 to tri- and di-methylated H3K27 peptides.

To further study the binding properties of the BDT1-BAH domain with methylated H3K27 peptides, we performed surface plasmon resonance (SPR) assays. SPR revealed a rapid and stable association of the BDT1-BAH-GST protein with tri- and di-methylated H3K27 peptides but not with unmethylated H3 peptides. BDT1-BAH had a strong binding affinity of 1.49 μM for the H3K27me3 peptide; the binding affinity dropped to 1.76 μM for the H3K27me2 peptide; and no binding affinity was detected for the unmethylated H3 peptide (Figure 2C-E). When the mutated aromatic cage protein BDT1-BAH-WY-m-GST was used, no

binding affinity was detected for any of the tested peptides (Figure 2F-H), which corroborated the results obtained from peptide pull-down assays. We also tested the binding ability of BDT1 with methylated H3K4, H3K9, and H3K36 peptides using peptide pull-down assays. Although BDT1 could also bind to methylated H3K9 peptides, the binding affinity of BDT1 was significantly stronger with H3K27me3 peptides than with methylated H3K9 peptides (Figure S3A, B), supporting the notion that BDT1 specifically recognizes H3K27me3.

BDT1 represses the expression of flowering genes

The previously reported *ebs* and *shl* mutants showed early flowering under long-day conditions (Li et al., 2018; Qian et al., 2018; Yang et al., 2018). The depletion of *BDT1* gene also significantly accelerates the flowering time compared to the WT Col-0 under long-day conditions (Figure 3A, B). Although wild-type *BDT1* complemented the early flowering phenotype of *bdt1*, the mutated aromatic cage gene *BDT1-WY-m* failed to rescue *bdt1* (Figures 3A, 3B, S4A). These results suggest that BDT1 is responsible for preventing early flowering and that the binding of H3K27me3 by the BAH domain is involved in the regulation of flowering time by BDT1.

To explore the molecular basis of BDT1 control of flowering time, we performed RNA-seq using 10-day-old seedlings grown under long-day conditions. We found that the expression of 432 genes was significantly changed ($\log_2$ (fold change)>1 or <-1; FDR<0.05) in the *bdt1* mutant. Among the differentially expressed genes in the *bdt1* mutant, 329 (76%) were up-regulated, and only 103 (24%) were down-regulated (Figure 5A). Gene Ontology (GO) analysis indicated that the up-regulated genes showed enrichment in GO terms related to post-embryonic development and reproductive development (Figure 5B). These up-regulated genes in the *bdt1* mutant included *FT* and a subset of MADS-box flowering genes,

i.e., *AGL6*, *SOC1*, and *FUL*. We performed quantitative RT-PCR (qRT-PCR) to further detect the expression levels of these flowering genes. Our results showed that the expression levels of these flowering genes were significantly increased in the *bdt1* mutant, while the expression levels were restored to the WT level in the complementation line (Figure 3C). Considering the recognition ability of BDT1 on H3K27me3, we then determined the H3K27me3 level of these flowering genes using published H3K27me3 deposition data (Zhou et al., 2017). All five genes showed H3K27me3 enrichment on their genic regions, and the enrichment was eliminated in the *clf swn* double mutant (Figure 3D). Nevertheless, the total H3K27me3 level was not altered in the *bdt1* mutant relative to the WT Col-0 (Figure S6). Next, we performed chromatin immunoprecipitation followed by quantitative PCR (ChIP-qPCR) to detect the enrichment of BDT1 at the genic regions of *AGL6*, *FT*, *FUL*, and *SOC1*. The results showed a 2- to 5-fold enrichment of BDT1 at these loci, and that the mutation of the aromatic cage disrupted the binding of BDT1 to these loci (Figure 3E). These results demonstrate that BDT1 binds to the H3K27me3-enriched flowering genes and represses the expression of these genes, thereby preventing early flowering.

We performed a dual luciferase reporter assay to determine whether BDT1 has transcriptional repression activity. As expected, the fusing of GAL4-BD with VP16, which is a strong transcriptional activator, increased the relative expression level of the luciferase reporter. The relative expression level of the luciferase reporter was significantly lower, however, when GAL4-BD was fused with both VP16 and BDT1 rather than with VP16 alone (Figure 3F). This indicates that the BDT1 protein acts as a transcriptional repressor *in vivo*, which is consistent with the finding that most of the differentially expressed genes are up-regulated in the *bdt1* mutant.

Given that *FT* and *SOC1* are key flowering genes, we investigated whether the early-flowering phenotype is caused by the up-regulation of *FT* and *SOC1* in the *bdt1* mutant. We introduced *ft* and/or *soc1* mutations into *bdt1* by genetic crossing and obtained the *bdt1 ft* and *bdt1 soc1* double mutants and the *bdt1 ft soc1* triple mutant. We found that while the *bdt1 ft* and *bdt1 soc1* double mutants flowered later than *bdt1*, they still flowered earlier than *ft* and *soc1*, respectively. The *bdt1 ft soc1* triple mutant, however, showed no difference with *ft soc1* double mutant, suggesting the depletion of both *FT* and *SOC1* completely rescued the early flowering phenotype of *bdt1* (Figures 3G, 3H, 3I, S7A, S7B). These genetic results further demonstrate that BDT1 regulates flowering time through these flowering genes.

BDT1 associates with a family of PHD finger-containing proteins via the BAH-PHD domain interaction

To identify the proteins that interact with BDT1, we performed immunoprecipitation followed by mass spectrometry (IP-MS) using *BDT1-FLAG* transgenic plants in the *bdt1* mutant background. By IP-MS, we identified six PHD domain-containing proteins that were co-purified with BDT1 (Figure 4A). BDT1 and one of the six PHD domain-containing proteins, which we named PHD domain-containing protein 1 (PHD1/AT1G43770) were previously reported to be co-purified with MOM1 (Han et al., 2016). We named the other five PHD domain-containing proteins as PHD domain-containing protein 2 (PHD2/AT5G16680/PAIPP2), 3 (PHD3/AT3G02890/AIPP2), 4 (PHD4/AT5G61110), 5 (PHD5/AT5G61100), and 6 (PHD6/AT5G61120). Alignment of the PHD domains of these proteins revealed a high degree of similarity, and the conserved C4HC3 motif existed in all the six proteins (Figure S8A). A phylogenetic tree showed high homology between PHD2 and PHD3, as

well as between PHD4 and PHD5 (Figure S8B). Interestingly, the C-TERMINAL DOMAIN PHOSPHATASE-LIKE2 (CPL2) was also co-purified with BDT1 (Figure 4A). CPL2 is a plant-specific Pol II carboxyl terminal domain (CTD)-Ser5 phosphatase (Koiwa et al., 2004), and is associated with transcription initiation (Hajheidari et al., 2013; Heidemann et al., 2013; Zaborowska et al., 2016). The *Arabidopsis cpl2* mutant exhibits pleiotropic defects in development and stress response, including early flowering, low fertility, leaf expansion defects, and increased salt sensitivity (Ueda et al., 2008). Next, we generated *PHD1-FLAG* transgenic plants in the WT Col-0 background and performed IP-MS. The IP-MS results showed that BDT1 was co-purified with PHD1-FLAG (Figure 4A). The interaction of BDT1 and PHD1 was confirmed by co-immunoprecipitation (co-IP) assay using transgenic plants harboring *BDT1-MYC* and/or *PHD1-FLAG* transgenes (Figure 4B). We also found that PHD2, PHD3, PHD4, PHD5, and PHD6 were not co-purified with PHD1-FLAG (Figure 4A), suggesting that BDT1 interacts with only one copy of the PHD domain-containing proteins in *Arabidopsis*.

We next performed yeast two-hybrid (Y2H) assays to detect the interaction between BDT1 and PHD proteins. Besides the full-length BDT1 (1-587 aa) and PHD1 (1-431 aa) proteins, we also used their truncated fragments to determine the domain requirement. The BDT1 protein was truncated into five fragments, including the BDT1 N-terminus with (1-273 aa) or without (1-94 aa) the BAH domain, the BAH cassette containing the BAH domain (95-273 aa), and the BDT1 C-terminus with (95-587 aa) or without (274-587 aa) the BAH domain. The PHD1 protein was also truncated into two fragments including the PHD1 N-terminus containing the PHD domain (1-100 aa), and the PHD1 C-terminus (101-431 aa) (Figure 4C). The Y2H results showed that the full-length of BDT1 and the BDT1 fragments that included the BAH domain (1-587 aa, 1-273 aa, 95-587 aa, and

95-273 aa) were capable of interacting with the full-length PHD1 (1-431 aa) or the PHD domain of PHD1 (1-100 aa). The BDT1 fragments without the BAH domain (1-94 aa or 274-587) could not interact with any PHD1 fragments or with the full-length PHD1 (Figures 4C, S9A). These results indicated that the BAH domain and the PHD domain are responsible for the interaction between BDT1 and PHD1. The interaction between BDT1-BAH (95-587 aa) and PHD1-PHD (1-100 aa) as determined by Y2H further demonstrated that the BAH and PHD domains are essential for the BDT1-PHD1 interaction. The Y2H results also showed that the BAH domain of BDT1 was able to interact with the PHD domain of PHD2/3/4/5/6 (Figures 4D, S9B). Thus, the BAH domain and the PHD domains mediate the interactions between BDT1 and all six PHD proteins (Figure 4E). Our *in vitro* pull-down assay using BDT1-His and PHD2-PHD-GST indicated that BDT1 directly interacts with the PHD proteins (Figure 4F). The aromatic cage in the BAH domain of BDT1 is responsible for binding to H3K27me3; mutations of the aromatic cage disrupted the binding of BAH to H3K27me3 (Figure 2A-H). However, the mutations of the aromatic cage did not influence the interaction between the BAH domain and the PHD domains (Figure S10A, B), suggesting that certain other residues in the BAH domain are responsible for the interaction of BDT1 with the PHD proteins.

The PHD domain increases the binding affinity of the BAH domain for H3K27me3

To explore the function of the BAH-PHD domain interaction, we performed histone peptide pull-down assays using BDT1-BAH-GST and PHD2-PHD-GST proteins. Although the PHD2-PHD-GST protein had no significant binding affinity for methylated H3K27 peptides, pre-incubation of PHD2-PHD-GST with BDT1-BAH-GST significantly increased the binding affinity for the methylated

H3K27 peptide, compared to BDT1-BAH-GST alone (Figure 5A). However, the pre- incubation of PHD2-PHD-GST with the mutated aromatic cage protein BDT1-BAH-WY-m-GST had no effect on the binding affinity for methylated H3K27 peptides (Figure 5B). To quantify the reinforcement of the PHD domain, we performed SPR assays in order to further study the effect of the PHD domain on the binding of BDT1-BAH to the methylated H3K27 peptide. The SPR assay showed that pre-incubated BDT1-BAH-GST and PHD2-PHD-GST proteins had a stronger binding affinity for H3K27me3 (64.9 nM) and H3K27me2 (118 nM) peptides than the BDT1-BAH-GST protein alone (Figures 5C, 5D, S11A, S11C). No binding affinity was detected between the PHD2-PHD-GST protein and any of the tested histone peptides (Figures 5D, 5G, S11B), which is consistent with the results of our peptide pull-down assay. Moreover, pre-incubation of PHD2-PHD-GST with BDT1-BAH-GST did not enhance the binding affinity of BDT1-BAH-GST for unmethylated H3 peptide in the SPR assay (Figure 5F, G, H). Of note, the binding affinities of BDT1-BAH for methylated H3K27 as determined by two independent SPR assays showed a little difference (Figures 2C, 2D, 5C, S11A), which is most likely to be caused by the use of different batches of the BDT1-BAH-GST protein or different SPR chips. Because the same batch of proteins and the same SPR chip were used in each of the SPR assays, the SPR results are sufficient to support the effects of the BAH mutations and of the addition of PHD2-PHD-GST on the affinity of BDT1-BAH for methylated H3K27. Together, the results suggest that the binding affinity of the BAH domain for the methylated H3K27 peptide is increased by the PHD domain.

PHD proteins repress the expression of flowering genes

To explore the biological function of the PHD proteins, we obtained available T-DNA mutants of PHD proteins and found that these mutants had no obvious

developmental defects (data not shown), suggesting that the PHD proteins are functionally redundant. We therefore generated a *phd1*/*2*/*3*/*4*/*5*/*6* sextuple mutant by CRISPR-Cas9-mediated mutagenesis in the *phd3* T-DNA mutant (SALK_057771) background (Figure S12A-E). Like the *bdt1* mutant, the *phd1*/*2*/*3*/*4*/*5*/*6* mutant exhibited early flowering under long-day conditions (Figure 6A, B). However, we also observed a growth retardation of the *phd1*/*2*/*3*/*4*/*5*/*6* mutant, which resulted in pleiotropic developmental defects including a smaller size and a lower fertility relative to the WT Col-0 (Figure 6C). The *bdt1* mutant was also slightly smaller than the WT, suggesting that BDT1 and the PHD proteins cooperate to regulate development-related phenotypes (Figure 6D). The up-regulated genes in the *bdt1* mutant are enriched in development-related GO terms, which is consistent with the developmental phenotypes observed in the *bdt1* mutant (Figure S5B). Although more severe developmental defects were observed in the *phd1*/*2*/*3*/*4*/*5*/*6* mutant than in the *bdt1* mutant, the flowering-time phenotype of the *phd1*/*2*/*3*/*4*/*5*/*6* mutant was even weaker than that of the *bdt1* mutant (Figure 6A-D). We suspected that the growth retardation in the *phd1*/*2*/*3*/*4*/*5*/*6* mutant may antagonize the early-flowering phenotype. Using qRT-PCR, we found that the expression levels of the selected flowering genes *AGL6* and *SOC1* were significantly increased in the *phd1*/*2*/*3*/*4*/*5*/*6* mutant relative to the WT Col-0. ChIP-qPCR showed that the PHD3 protein was enriched at the genic regions of *AGL6* and *SOC1* (Figure 6C). These results support the notion that, like BDT1, the PHD proteins can also associate with the flowering genes and thereby suppress their transcription.

DISCUSSION

In this study, we identified an H3K27me3 reader protein, BDT1, which cooperates with PHD proteins to repress a group of flowering genes. BDT1 recognizes

H3K27me3 markers through a conserved BAH domain that was also previously reported to be present in EBS and SHL (Li et al., 2018; Qian et al., 2018; Yang et al., 2018). In the conserved BAH domain, the aromatic cage composed of Tyr149, Trp170, and Tyr172 is required for binding to H3K27me3. Unlike the EBS and SHL proteins, which harbor both the BAH and PHD domains, the BDT1 protein lacks the PHD domain. Our IP-MS and *in vitro* binding assays, however, revealed that BDT1 interacts with several PHD domain-containing proteins (Figure 4A, B, E). Thus, these PHD proteins may complement the lack of PHD in BDT1. We previously found that MOM1 and PIAL2 interact and form a complex that is responsible for transcriptional silencing and that the fusing of the MOM1 protein with the PIAL2 proteins completely restore the transcriptional silencing in the *mom1 pial2* double mutant (Zhao and He, 2018). In the future, it will be interesting to determine whether the fusing of BDT1 with each of the PHD proteins mimics the *in vivo* interaction.

CPL2, a phosphatase of Pol II CTD-Ser5 (Koiwa et al., 2004), was co-purified with BDT1 (Figure 4A). The phosphorylation of Pol II CTD-Ser5 is associated with transcription initiation, which aids in promoter escape and recruitment of RNA-5'-end-capping machinery (Hajheidari et al., 2013; Heidemann et al., 2013; Zaborowska et al., 2016). Because of the interaction between BDT1 and CPL2, we suspected that the depletion of BDT1 may cause disassociation of CPL2 from Pol II CTD-Ser5 on BDT1 target loci and then lead to de-repression of these target genes. Consistent with that assumption, the early-flowering phenotype was evident in the *cpl2* mutant (Ueda et al., 2008), suggesting that the regulation of flowering time by BDT1 is related to CPL2. Considering that both the PHD proteins and CPL2 were co-purified with BDT1 (Figure 4A), and given that the developmental defects were more severe in the *phd1/2/3/4/5/6* mutant than in the *bdt1* mutant (Figure 6C, 6D), we propose that the PHD proteins may form a

protein complex not only with BDT1 but also with other proteins, such as CPL2, in order to mediate transcriptional repression. BDT1 is mainly responsible for recruiting the complex to H3K27me3-enriched genomic loci. Because the PHD domains are thought to interact with multiple histone markers (Li and Li, 2012; Zhao et al., 2018), the PHD proteins by themselves may associate with the Arabidopsis genome more extensively than BDT1. Depletion of BDT1 may cause mis-deposition only of the complex on chromatin. However, depletion of the PHD proteins not only disrupts the deposition of the complex on certain specific chromatin loci but also disrupts the association of the PHD domains with the chromatin loci that are not bound by the complex, thus leading to more severe developmental defects.

When we were preparing this manuscript, we learned that a similar work was recently published (Zhang et al., 2020). Although most of the results reported by Zhang et al. were confirmed by the current study, the current study includes two additional major findings that were not previously reported. First, all six members of the PHD family were co-purified with BDT1 (Figure 4A). In Zhang et al. (2020), in contrast, only two PHD family members, PHD3 and PHD2 were co-purified with BDT1. Moreover, the interactions of BDT1 with the six PHD proteins were all confirmed by the Y2H assay in the current study (Figure 4C-E). Our results suggest that each of the PHD proteins independently interacts with BDT1 and then forms multiple redundant BDT1-PHD complexes. Second, we found that the PHD domain can increase the binding affinity of the BAH domain for H3K27me3 (Figure 5A-K). Zhang et al. (2020) revealed a binding affinity of PHD2 to unmodified H3K4, which may contribute to the recruitment of the BDT1-PHD complex to the transcription-repressive H3K4me3-depletion region (Zhang et al., 2020). Their research, however, did not reveal whether and how BDT1 cooperates with the PHD proteins in the redundant BDT1-PHD complexes

to bind to the K3K27me3 peptide. In our study, we simultaneously incubated BAH and PHD with either H3K27-methylated or non-methylated peptides and found that the PHD domain can enhance the binding of the BAH domain to H3K27-methylated peptides but not to non-methylated peptides. Our results therefore strongly support the inference that the BAH and PHD domains can function as a whole in the BDT1-PHD complexes to recognize the H3K27me3 peptide.

The reinforcement of the binding to modified histone by the cooperation of two individual domains has been previously demonstrated. In humans, the PHD domain of Pygo1 can bind to H3K4me2, and the binding affinity of the Pygo1 PHD for methylated H3K4 peptides was enhanced by the homology domain 1 (HD1) of BCL9 (Fiedler et al., 2008). Our recent study showed that, ARID5, which is an accessory subunit of the *Arabidopsis* ISWI chromatin-remodeling complex, binds to the H3K4me3 peptide through a PHD domain, and that an ARID domain adjacent to the PHD domain can help the binding of ARID5 to the H3K4me3 peptide (Tan et al., 2020). Dual recognition of modified histone by two individual domains may therefore be a common mechanism in eukaryotes. Determining how the PHD domain reinforces the binding of BDT1 to H3K27-methylated histone in detail will require additional research on the structure of the BDT1-PHD-H3K27me3 ternary complex.

MATERIALS AND METHODS

Plant materials and growth conditions

The T-DNA insertion mutants *bdt1* (GK-058D11), *phd3* (SALK_057771), *ft* (GK_290E08), *soc1* (SALK_138131), and *clf* (SALK_088542) were obtained from the Arabidopsis Biological Resource Center (ABRC). The *bdt1 ft* and *bdt1*

soc1 double mutants and the *bdt1 ft soc1* triple mutant were generated by crossing. The *phd1*/*2*/*3*/*4*/*5*/*6* sextuple mutant was generated by CRISPR/Cas9-mediated mutagenesis in the *phd3* mutant background. All of the mutants were in the Col-0 background. Primers used for mutagenesis and sequence are listed in Dataset S5.

The full-length genomic sequences of the WT *BDT1*, *PHD1*, *PHD3*, and the mutated *BDT1* (for producing W170L and Y172A mutations) without the stop codon driven by their native promoter were introduced into *pCAMBIA1305* vectors with *FLAG* or *GFP* tags and/or *pRI909* vector with MYC tag. The constructs were transformed into Agrobacterium strain *GV3101* and were then introduced into Col-0 plants or corresponding mutant plants by the floral-dip method to generate epitope-tagged transgenic plants. The T1 seedlings were grown on MS medium supplemented with 30 mg/L Hygromycin, 50 mg/L Ampicillin (for *pCAMBIA 1305*) or 150 mg/L Kanamycin, 50 mg/L Ampicillin (for *pRI909*). The *BDT1-MYC PHD1-FLAG* plants were generated by crossing *BDT1-MYC* and *PHD1-FLAG* transgenic plants in the Col-0 background. Primers used for the construction are listed in Dataset S5. Seeds were sown on Murashige and Skoog (MS) medium plates, and seedlings were grown at 22°C under long-day conditions (16 h light/8 h dark). The seedlings were transplanted into soil and grown under the same conditions for assessment of flowering time and plant height.

Affinity purification, mass-spectrometric analysis, co-immunoprecipitation, and peptide affinity purification

For affinity purification, 3 g of inflorescence tissue was ground in liquid nitrogen and homogenized in 15 mL of lysis buffer (50 mM Tris-HCl, pH 7.6, 150 mM NaCl, 5 mM $MgCl_2$, 10% glycerol, 0.1% NP-40, 1 mM DTT, 1 mM PMSF, and 1% Roche protease inhibitor cocktail tablet) for 10 min at 4℃. After

centrifugation two times at 18,407 *g* for 15 min at 4°C, the supernatant was passed through two layers of miracloth, and the filtrate was incubated with 100 μL of anti-FLAG M2 Affinity Gel beads (Sigma, A2220) for 2.5 h at 4°C with rotation. After they were washed five times with lysis buffer, the protein-bound beads were eluted with 3 μL of 3× FLAG peptide (Sigma, F4799). The eluted proteins were run on an SDS-PAGE gel and then subjected to MS analysis as previously described (Tan et al., 2020).

For co-immunoprecipitation, 1 g of the inflorescence tissue from the *BDT1-MYC PHD1-FLAG* plants and *BDT1-MYC* transgenic plants was subjected to affinity purification using 100 μL of anti-FLAG M2 Affinity Gel beads. The input and eluted proteins were run on an SDS-PAGE gel for immunoblotting and were detected by anti-FLAG (Sigma, F1804) and anti-MYC (Abmart, M20002) antibodies diluted at 1:5000.

Peptide affinity purification was performed as previously described (Zhang et al., 2018). In brief, 1 g of the inflorescence tissue was ground and homogenized in 15 mL of Honda Buffer (20 mM HEPES-KOH, pH 7.4, 0.44 M sucrose, 1.25% ficoll, 2.5% Dextran T40, 10 mM $MgCl_2$, 0.5% Triton X-100, 1 mM DTT, 1 mM PMSF, and 1% Roche protease inhibitor cocktail tablet) for 10 min at 4°C before it was passed through two layers of miracloth. After the filtrate was centrifuged at 2,000 *g* for 15 min at 4°C, the nuclear pellets were washed two times with 1 mL of Honda buffer and were resuspended in 600 μL of Nuclei Lysis Buffer (50 mM Tris-HCl, pH 8.0, 150 mM NaCl, 1% NP40, 0.5 mM DTT, 1 mM PMSF, and 1% Roche protease inhibitor cocktail tablet); the pellets were then sonicated with a Bioruptor (Diagenode). After the sonicated pellets were centrifuged at 20,000 *g* for 10 min at 4°C, the supernatant was incubated with 2 μg of biotinylated histone peptides (H3K27me3 or H3 peptide respectively) for 3 h at 4°C with rotation. The

mixture was then incubated with 40 μL of Streptavidin MagneSphere Paramagnetic Particles (Promega, Z5481) for 1 h at 4°C with rotation. The particles were washed three times with wash buffer 1 (320 mM NaCl, 50 mM Tris-HCl, pH 8.0, and 0.5% NP-40) and three times with wash buffer 2 (150 mM NaCl, and 50 mM Tris-HCl, pH 8.0). The beads were then boiled in SDS sample buffer. The proteins were subjected to MS analysis or were detected by immunoblotting using anti-FLAG antibody diluted at 1:5,000.

Comparative modeling

Comparative modeling of BDT1-BAH was performed using the template of EBS-BAH (PDB ID: 5Z8L). Modeled structure was verified with 10-ns molecular dynamics (MD) simulation using GROMACS (AMBER force field). H3 peptide structure was generated manually and then energy-minimized with Protein Local Optimization Program (PLOP). The peptide was then docked into the BDT1-BAH domain surface using the Flexpep Dock Server, and the 10 complex structures with the highest scores were saved as candidates. The docked complex structures were then energy-minimized with PLOP and one manually picked candidate structure was saved as final model structure. Structure views shown in figures were edited with UCSF CHIMERA.

Protein expression, purification, and pull-down

The full-length or BAH cassette of the WT or mutated *BDT1* coding sequences and the PHD cassette of PHD2 coding sequence were cloned and constructed into pET28a and/or pGEX6p-1 vectors with 6×His or GST tags fused to their N-terminals. The plasmids were then transformed into the *Escherichia coli* strain Transetta (DE3) (TRAN, M651123). When the OD_{600} of the bacteria reached 0.6-0.8, protein expression was induced at 16°C overnight with 0.3 mM IPTG.

After bacterial suspensions were centrifuged, the pelleted bacteria were resuspended in His lysis buffer (20 mM Tris-HCl, pH 7.8, 500 mM NaCl, and 20 mM imidazole) or GST lysis buffer (20 mM Tris-HCl, pH 7.5, and 150 mM NaCl), and then were sonicated for 3 min. After the preparation was centrifuged at 18,000 g for 1 h at 4°C, the supernatant was passed through a 0.45-μm microfiltration membrane, and the filtrate was incubated with Ni-NTA His·Bind Resin (Millipore, 70666) or glutathione-sepharose 4B (GE Healthcare, 17075601). After they were washed with lysis buffer, the bead-bound proteins were eluted using His elution buffer (20 mM Tris-HCl, pH 7.8, 500 mM NaCl, and 250 mM imidazole) or GST elution buffer (50 mM Tris-HCl, pH 7.5, 150 mM NaCl, and 10 mM glutathione).

For the pull-down assay, 1 μg of BDT1-His protein was incubated with 1 μg of PHD2-PHD-GST protein in 600 μL of GST lysis buffer for 2 h at 4°C with rotation. The mixture was incubated with 30 μL of glutathione-sepharose 4B beads for 1 h at 4°C with rotation. After they were washed 5 times with 1 mL of GST lysis buffer, the protein-bound beads were boiled in SDS sample buffer. The input and pull-down samples were run on an SDS-PAGE gel for immunoblotting by anti-GST (Abmart, M20007L) or anti-His (ORIGENE, TA100013) antibodies diluted at 1:5,000.

Histone peptide pull-down

A 1-μg quantity of recombinant proteins was incubated with 1 μg of biotinylated histone peptides in 600 μL of binding buffer (50 mM Tris-HCl, pH 7.5, 150 mM NaCl, and 0.05% NP-40) for 4 h at 4°C with rotation. The recombinant proteins without the histone peptides were used as negative controls. For the simultaneous incubation of BDT1-BAH-GST and PHD2-PHD-GST proteins, the two proteins were pre-incubated for 2 h before they were added to the biotinylated histone

peptides. The mixture was then incubated with 20 μL of Streptavidin MagneSphere Paramagnetic Particles for 1 h at 4°C with rotation. After they were washed with binding buffer, the protein-bound beads were boiled in SDS sample buffer and were subjected to immunoblotting using anti-GST or anti-His antibodies diluted at 1:5,000. The histone peptides H3 (21-44 aa), H3K27me1 (21-44 aa), H3K27me2 (21-44 aa), H3K27me3 (21-44 aa), H3K4me1 (1-21 aa), H3K4me2 (1-21 aa), H3K4me3 (1-21 aa), and H3K9me1 (1-21 aa) were synthesized (Beijing Scilight Biotechnology LLC). Other histone peptides used in this study were H3K9me2 (Active Motif, 810406), H3K9me3 (Active Motif, 810407), H3K36me1 (EpiCypher, 12-0022), H3K36me2 (EpiCypher, 12-0023), and H3K36me3 (EpiCypher, 12-0024).

Surface plasmon resonance assays

The surface plasmon resonance (SPR) assays were performed at 25°C using a BIAcore T200 instrument (GE Healthcare). The streptavidin molecules were immobilized on a Sensor Chip CM5 (GE Healthcare, BR-1005-30) using the amine coupling kit according to the manufacturer's instructions (GE Healthcare). The same amounts of biotinylated histone peptides H3K27me3, H3K27me2, and H3 (640 RU for H3K27me3, 650 RU for H3K27me2, and 640 RU for H3) were then captured on the chip. The protein samples were prepared in running buffer (411 mM NaCl, 8.1 mM KCl, 30 mM Na_2HPO_4, 5.4 mM KH_2PO_4, and 0.1% Tween-20), and were serially diluted (2-fold) before injection. After each association and dissociation cycle, surfaces were regenerated with 5 M NaCl buffer. Data were analyzed with Biacore T200 Evaluation Software, and the two state reaction fitting model was used to fit the original curves.

RNA transcript analysis

For RNA-seq, 1-g quantities of 10-day-old seedlings of Col-0 and *bdt1* were collected and ground in liquid nitrogen. Total RNA was extracted using Trizol reagent (Invitrogen) and was then sent to Vazyme Biotech for reverse transcription and library construction. The libraries were sequenced with an Illumina HiSeqXTen instrument using a paired-end scheme (PE150). The clean reads were mapped to the Arabidopsis genome (TAIR10) using the HISAT version 2.2.0 program (Kim et al., 2019). The featureCounts version 2.0.0 was used to perform genetic quantitative analysis on unique mapping readings (Liao et al., 2014). The R package edgeR version 3.28.1 was used to identify differentially expressed genes (DEGs) in transcriptome sequencing data (Robinson et al., 2010). Normalization was performed using TMM method, and the dispersion estimates were calculated by estimateCommonDisp and estimateTagwiseDisp functions. The exact test was achieved through edgeR's exactTest function, and the DEGs were screening by $\log_2$ (fold change)>1 or <-1 and FDR<0.05. In order to explore the function of DEGs, the R package clusterProfiler version 3.14.3 was used for functional analysis (Yu et al., 2012). For qRT-PCR, 0.1-g quantities of 10-day-old seedlings were collected and ground in liquid nitrogen. Total RNA was extracted using Trizol reagent (Invitrogen), and cDNA was synthesized using the One-Step gDNA Removal reverse transcription kit (Transgene, AE341-02). The cDNA was used for RT-qPCR using KAPA SYBR FAST qPCR Master Mix (KAPA, KR0389). Primers used for RT-qPCR are listed in Supplementary Dataset S5.

Chromatin immunoprecipitation

BDT1-GFP and mutated *BDT1-WY-m-GFP* (W170L and Y172A) transgenic plants in the *bdt1* background and *PHD3-FLAG* transgenic plants in the Col-0

background were used for ChIP; *bdt1* mutant or the WT Col-0 plants were used as negative controls.

After 2-g quantities of 10-day-old seedlings were fixed with 1% formaldehyde (Sigma, F8775), the samples were ground and homogenized in 20 mL of NEB1 buffer (10 mM Tris-HCl, pH 8.0, 0.4 M sucrose, 10 mM $MgCl_2$, 1 mM DTT, 1 mM PMSF, and 1% Roche protease inhibitor cocktail tablet). The homogenate was passed through two layers of miracloth, and the filtrate was centrifuged at 1,986 g for 20 min at 4°C. After the preparation was washed 4 times with NEB2 buffer (10 mM Tris-HCl, pH 8.0, 0.25 M sucrose, 10 mM $MgCl_2$, and 1% Triton X-100), the nuclei in the pellet were resuspended in 500 μL of NEB3 buffer (10 mM Tris-HCl, pH 8.0, 1.7 M sucrose, 2 mM $MgCl_2$, 0.15% Triton X-100, 1 mM PMSF, and 1% Roche protease inhibitor cocktail tablet), and were then loaded on top of 500 μL of NEB3 buffer in centrifuge tubes. After centrifugation at 15,871 g for 1 h at 4°C, the pellet was resuspended in 600 μL of nuclear lysis buffer (20 mM Tris-HCl, pH8.0, 2 mM EDTA, 0.2% NP-40, 0.25% SDS, 1 mM PMSF, and 1% Roche protease inhibitor cocktail tablet), and was subjected to sonication. After the sample was centrifuged at 16,000 g for 15 min at 4°C, the supernatant was diluted 4-fold with dilution buffer (20 mM Tris-HCl, pH8.0, 2 mM EDTA, 200 mM NaCl, 1 mM PMSF, and 1% Roche protease inhibitor cocktail tablet). The chromatin was immunoprecipitated using laboratory-prepared GFP beads or Anti-FLAG M2 Magnetic Beads (SIGMA, M8823). The beads were washed, and the protein-DNA complex was eluted with elution buffer (0.1% SDS and 0.1 M $NaHCO_3$) and was then reverse cross-linked at 65°C and treated with proteinase K and RNase. The DNA was then purified for quantitative PCR. Primers used for ChIP-qPCR are listed in Dataset S5.

Dual luciferase reporter assay

For the dual luciferase reporter assay, a firefly luciferase reporter gene driven by a minimal 35S promoter with a GAL4-BD binding site（*5×UAS*) was used as the reporter vector. The Renilla luciferase reporter gene driven by a constitutive promoter was used as the reference vector. The effector vector contained a 35S promoter-driven GAL4-DNA- binding domain (GAL4-BD), which was fused with VP16 or with both VP16 and BDT1. The effector vector containing only GAL4-BD was used as the control. The reporter vector, reference vector, and effector vector were transformed into Arabidopsis mesophyll protoplasts as previously described (Yoo et al., 2007). Luciferase activity was measured using the Dual-Luciferase Reporter Assay System (E1910, Promega) in a Promega GloMax 20/20 luminometer.

Yeast two-hybrid assay

The full-length or truncated coding sequences of the *BDT1* (WT or WY-m mutated) and *PHD1-6* genes were cloned into the pGADT7 and/or pGBKT7 vectors to generate AD and BD constructs, respectively. The AD and BD constructs were then transformed into the yeast strains AH109 and Y187, respectively. After mating, Y2H assays were performed on synthetic dropout (SD) medium lacking tryptophan (Trp), leucine (Leu), and histidine (His) but supplemented with 3 mM 3-amino-1,2,4-triazol (3-AT). Primers used for construction are listed in Dataset S5.

Histone immunoblotting

A 0.5-g quantity of 10-day-old seedlings was ground and homogenized in 10 mL of nuclear isolation buffer (20 mM Tris-HCl, pH 7.5, 25% glycerol, 20 mM KCl, 2 mM EDTA, 2.5 mM $MgCl_2$, 0.25 M sucrose, and 5 mM DTT). After passage

through two layers of miracloth, the filtrate was centrifuged at 1,500 g for 15 min at 4˚C and was then washed 4 times with NRBT buffer (20 mM Tris-HCl, pH 7.5, 2.5 mM $MgCl_2$, 25% glycerol, and 0.2% Triton X-100). The nuclei were boiled with SDS loading buffer and were subjected to immunoblotting using anti-H3K27me3 (1:2,000 dilution) or anti-H3 (1:10,000 dilution) antibodies.

Accession numbers

Sequence data used in this study are from TAIR 10. The accession numbers are as follows: *BDT1*/*AIPP3* (AT4G11560), *PHD1* (AT1G43770), *PHD2*/*PAIPP2* (AT5G16680), *PHD3*/*AIPP2* (AT3G02890), *PHD4* (AT5G61110), *PHD5* (AT5G61100), *PHD6* (AT5G61120), *CPL2* (AT5G01270), *FT* (AT1G65480), *SOC1* (AT2G45660), *AGL6* (AT2G45650), *FUL* (AT5G60910), *CLF* (AT2G23380), *SWN* (AT4G02020).

ACKNOWLEDGEMENTS

This work was supported by the National Natural Science Foundation of China (32025003) and by the National Key Research and Development Program of China (2016YFA0500801) from the Chinses Ministry of Science and Technology.

AUTHOR CONTRIBUTIONS

F.Q. and X.J.H. designed the experiments, analyzed the data, and wrote the manuscript. F.Q., Q.Y.Z, T.N.Z, Y.L.L., L.L., J.H.S, and S.C. performed the experiments. Y.N.S. performed the bioinformatics analysis. All authors read and approved of the manuscript.

DATA AVAILABILITY

Raw RNA-seq data have been deposited in the Gene Expression Omnibus (GEO) database with the accession code GSE164325.

REFERENCES

Aasland, R., Gibson, T.J., and Stewart, A.F. (1995). The PHD finger: Implications for chromatin-mediated transcriptional regulation. Trends Biochem. Sci. **20:** 56-59.

Amasino, R. (2010). Seasonal and developmental timing of flowering. Plant J. **61:** 1001-1013.

Balanza, V., Martinez-Fernandez, I., Sato, S., Yanofsky, M.F., and Ferrandiz, C. (2019). Inflorescence meristem fate is dependent on seed development and FRUITFULL in *Arabidopsis thaliana.* Front. Plant Sci. **10:** 1622.

Balanza, V., Martinez-Fernandez, I., Sato, S., Yanofsky, M.F., Kaufmann, K., Angenent, G.C., Bemer, M., and Ferrandiz, C. (2018). Genetic control of meristem arrest and life span in *Arabidopsis* by a FRUITFULL-APETALA2 pathway. Nat. Commun. **9:** 565.

Bratzel, F., Lopez-Torrejon, G., Koch, M., Del Pozo, J.C., and Calonje, M. (2010). Keeping cell identity in *Arabidopsis* requires PRC1 RING-finger homologs that catalyze H2A monoubiquitination. Curr. Biol. **20:** 1853-1859.

Campos, E.I., and Reinberg, D. (2009). Histones: Annotating chromatin. Annu. Rev. Genet. **43:** 559-599.

Cao, R., Tsukada, Y., and Zhang, Y. (2005). Role of Bmi-1 and Ring1A in H2A ubiquitylation and *Hox* gene silencing. Mol. Cell **20:** 845-854.

Chambers, A.L., Pearl, L.H., Oliver, A.W., and Downs, J.A. (2013). The BAH domain of Rsc2 is a histone H3 binding domain. Nucleic Acids Res. **41:** 9168-9182.

Chanvivattana, Y., Bishopp, A., Schubert, D., Stock, C., Moon, Y.H., Sung, Z.R., and Goodrich, J. (2004). Interaction of Polycomb-group proteins controlling flowering in *Arabidopsis.* Development **131:** 5263-5276.

Chen, D.H., Huang, Y., Ruan, Y., and Shen, W.H. (2016). The evolutionary landscape of PRC1 core components in green lineage. Planta **243:** 825-846.

Cho, L.H., Yoon, J., and An, G. (2017). The control of flowering time by environmental factors. Plant J. **90:** 708-719.

Corbesier, L., Vincent, C., Jang, S., Fornara, F., Fan, Q., Searle, I., Giakountis, A., Farrona, S., Gissot, L., Turnbull, C., and Coupland, G. (2007). FT protein movement contributes to long-distance signaling in floral induction of *Arabidopsis*. Science **316:** 1030-1033.

Derkacheva, M., Steinbach, Y., Wildhaber, T., Mozgova, I., Mahrez, W., Nanni, P., Bischof, S., Gruissem, W., and Hennig, L. (2013). *Arabidopsis* MSI1 connects LHP1 to PRC2 complexes. EMBO J. **32:** 2073-2085.

Du, J., Zhong, X., Bernatavichute, Y.V., Stroud, H., Feng, S., Caro, E., Vashisht, A.A., Terragni, J., Chin, H.G., Tu, A., Hetzel, J., Wohlschlegel, J.A., Pradhan, S., Patel, D.J., and Jacobsen, S.E. (2012). Dual binding of chromomethylase domains to H3K9me2-containing nucleosomes directs DNA methylation in plants. Cell **151:** 167-180.

Fan, H., Lu, J., Guo, Y., Li, D., Zhang, Z.M., Tsai, Y.H., Pi, W.C., Ahn, J.H., Gong, W., Xiang, Y., Allison, D.F., Geng, H., He, S., Diao, Y., Chen, W.Y., Strahl, B.D., Cai, L., Song, J., and Wang, G.G. (2020). BAHCC1 binds H3K27me3 via a conserved BAH module to mediate gene silencing and oncogenesis. Nat. Genet. **52:** 1384-1396.

Ferrandiz, C., Gu, Q., Martienssen, R., and Yanofsky, M.F. (2000). Redundant regulation of meristem identity and plant architecture by FRUITFULL, APETALA1 and CAULIFLOWER. Development **127:** 725-734.

Fiedler, M., Sanchez-Barrena, M.J., Nekrasov, M., Mieszczanek, J., Rybin, V., Muller, J., Evans, P., and Bienz, M. (2008). Decoding of methylated histone H3 tail by the Pygo-BCL9 Wnt signaling complex. Mol. Cell **30:** 507-518.

Hajheidari, M., Koncz, C., and Eick, D. (2013). Emerging roles for RNA polymerase II CTD in *Arabidopsis*. Trends Plant Sci. **18:** 633-643.

Han, Y.F., Zhao, Q.Y., Dang, L.L., Luo, Y.X., Chen, S.S., Shao, C.R., Huang, H.W., Li, Y.Q., Li, L., Cai, T., Chen, S., and He, X.J. (2016). The SUMO E3 ligase-like proteins PIAL1 and PIAL2 interact with MOM1 and form a novel complex required for transcriptional silencing. Plant Cell **28:** 1215-1229.

Heidemann, M., Hintermair, C., Voss, K., and Eick, D. (2013). Dynamic phosphorylation patterns of RNA polymerase II CTD during transcription. Biochim. Biophys. Acta **1829:** 55-62.

Hou, X., Zhou, J., Liu, C., Liu, L., Shen, L., and Yu, H. (2014). Nuclear factor Y-mediated H3K27me3 demethylation of the SOC1 locus orchestrates flowering responses of *Arabidopsis*. Nat. Commun. **5:** 4601.

Jaeger, K.E., and Wigge, P.A. (2007). FT protein acts as a long-range signal in *Arabidopsis*. Curr. Biol. **17:** 1050–1054.

Jing, Y., Guo, Q., and Lin, R. (2019). The B3-domain transcription factor VAL1 regulates the floral transition by repressing FLOWERING LOCUS T. Plant Physiol. **181:** 236–248.

Jung, J.H., Ju, Y., Seo, P.J., Lee, J.H., and Park, C.M. (2012). The SOC1-SPL module integrates photoperiod and gibberellic acid signals to control flowering time in *Arabidopsis*. Plant J. **69:** 577–588.

Kim, D., Paggi, J.M., Park, C., Bennett, C., and Salzberg, S.L. (2019). Graph-based genome alignment and genotyping with HISAT2 and HISAT-genotype. Nat. Biotechnol. **37:** 907–915.

Kohler, C., Hennig, L., Bouveret, R., Gheyselinck, J., Grossniklaus, U., and Gruissem, W. (2003a). *Arabidopsis* MSI1 is a component of the MEA/FIE Polycomb group complex and required for seed development. EMBO J. **22:** 4804–4814.

Kohler, C., Hennig, L., Spillane, C., Pien, S., Gruissem, W., and Grossniklaus, U. (2003b). The Polycomb-group protein MEDEA regulates seed development by controlling expression of the MADS-box gene *PHERES1*. Genes Dev. **17:** 1540–1553.

Koiwa, H., Hausmann, S., Bang, W.Y., Ueda, A., Kondo, N., Hiraguri, A., Fukuhara, T., Bahk, J.D., Yun, D.J., Bressan, R.A., Hasegawa, P.M., and Shuman, S. (2004). *Arabidopsis* C-terminal domain phosphatase-like 1 and 2 are essential Ser-5-specific C-terminal domain phosphatases. Proc. Natl. Acad. Sci. USA **101:** 14539–14544.

Lafos, M., Kroll, P., Hohenstatt, M.L., Thorpe, F.L., Clarenz, O., and Schubert, D. (2011). Dynamic regulation of H3K27 trimethylation during *Arabidopsis* differentiation. PLoS Genet. **7:** e1002040.

Li, S., Yang, Z., Du, X., Liu, R., Wilkinson, A.W., Gozani, O., Jacobsen, S.E., Patel, D.J., and Du, J. (2016). Structural basis for the unique multivalent readout of unmodified H3 tail by *Arabidopsis* ORC1b BAH-PHD cassette. Structure **24:** 486–494.

Li, Y., and Li, H. (2012). Many keys to push: Diversifying the 'readership' of plant homeodomain fingers. Acta Biochim. Biophys. Sin. (Shanghai) **44:** 28–39.

Li, Z., Fu, X., Wang, Y., Liu, R., and He, Y. (2018). Polycomb-mediated gene silencing by the BAH-EMF1 complex in plants. Nat. Genet. **50:** 1254–1261.

Liao, Y., Smyth, G.K., and Shi, W. (2014). featureCounts: An efficient general purpose program for assigning sequence reads to genomic features. Bioinformatics **30:** 923–930.

Liu, C., Lu, F., Cui, X., and Cao, X. (2010). Histone methylation in higher plants. Annu. Rev. Plant Biol. **61:** 395–420.

Musselman, C.A., and Kutateladze, T.G. (2011). Handpicking epigenetic marks with PHD fingers. Nucleic Acids Res. **39:** 9061–9071.

Piunti, A., and Shilatifard, A. (2016). Epigenetic balance of gene expression by Polycomb and COMPASS families. Science **352:** aad9780.

Qian, S., Lv, X., Scheid, R.N., Lu, L., Yang, Z., Chen, W., Liu, R., Boersma, M.D., Denu, J.M., Zhong, X., and Du, J. (2018). Dual recognition of H3K4me3 and H3K27me3 by a plant histone reader SHL. Nat. Commun. **9:** 2425.

Robinson, M.D., McCarthy, D.J., and Smyth, G.K. (2010). edgeR: A bioconductor package for differential expression analysis of digital gene expression data. Bioinformatics **26:** 139–140.

Schindler, U., Beckmann, H., and Cashmore, A.R. (1993). HAT3.1, a novel *Arabidopsis* homeodomain protein containing a conserved cysteine-rich region. Plant J. **4:** 137–150.

Searle, I., He, Y., Turck, F., Vincent, C., Fornara, F., Krober, S., Amasino, R.A., and Coupland, G. (2006). The transcription factor FLC confers a flowering response to vernalization by repressing meristem competence and systemic signaling in *Arabidopsis*. Genes Dev. **20:** 898–912.

Shafiq, S., Berr, A., and Shen, W.H. (2014). Combinatorial functions of diverse histone methylations in *Arabidopsis thaliana* flowering time regulation. New Phytol. **201:** 312–322.

Tan, L.M., Liu, R., Gu, B.W., Zhang, C.J., Luo, J., Guo, J., Wang, Y., Chen, L., Du, X., Li, S., Shao, C.R., Su, Y.N., Cai, X.W., Lin, R.N., Li, L., Chen, S., Du, J., and He, X.J. (2020). Dual recognition of H3K4me3 and DNA by the ISWI component ARID5 regulates the floral transition in *Arabidopsis*. Plant Cell **32:** 2178–2195.

Teper-Bamnolker, P., and Samach, A. (2005). The flowering integrator FT regulates SEPALLATA3 and FRUITFULL accumulation in *Arabidopsis* leaves. Plant Cell **17:** 2661–2675.

Turck, F., Roudier, F., Farrona, S., Martin-Magniette, M.L., Guillaume, E., Buisine, N., Gagnot, S., Martienssen, R.A., Coupland, G., and Colot, V. (2007). *Arabidopsis* TFL2/LHP1 specifically associates with genes marked by trimethylation of histone H3 lysine 27. PLoS Genet. **3:** e86.

Ueda, A., Li, P., Feng, Y., Vikram, M., Kim, S., Kang, C.H., Kang, J.S., Bahk, J.D., Lee, S.Y., Fukuhara, T., Staswick, P.E., Pepper, A.E., and Koiwa, H. (2008). The *Arabidopsis thaliana* carboxyl-terminal domain phosphatase-like 2 regulates plant growth, stress and auxin responses. Plant Mol. Biol. **67:** 683-697.

Xiao, J., Lee, U.S., and Wagner, D. (2016). Tug of war: Adding and removing histone lysine methylation in *Arabidopsis*. Curr. Opin. Plant Biol. **34:** 41-53.

Yang, C., Bratzel, F., Hohmann, N., Koch, M., Turck, F., and Calonje, M. (2013). VAL- and AtBMI1-mediated H2Aub initiate the switch from embryonic to postgerminative growth in *Arabidopsis*. Curr. Biol. **23:** 1324-1329.

Yang, N., and Xu, R.M. (2013). Structure and function of the BAH domain in chromatin biology. Crit. Rev. Biochem. Mol. Biol. **48:** 211-221.

Yang, Z., Qian, S., Scheid, R.N., Lu, L., Chen, X., Liu, R., Du, X., Lv, X., Boersma, M.D., Scalf, M., Smith, L.M., Denu, J.M., Du, J., and Zhong, X. (2018). EBS is a bivalent histone reader that regulates floral phase transition in *Arabidopsis*. Nat. Genet. **50:** 1247-1253.

Yoo, S.D., Cho, Y.H., and Sheen, J. (2007). *Arabidopsis* mesophyll protoplasts: a versatile cell system for transient gene expression analysis. Nat. Protoc. **2:** 1565-1572.

Yoo, S.K., Chung, K.S., Kim, J., Lee, J.H., Hong, S.M., Yoo, S.J., Yoo, S.Y., Lee, J.S., and Ahn, J.H. (2005). CONSTANS activates SUPPRESSOR OF OVEREXPRESSION OF CONSTANS 1 through FLOWERING LOCUS T to promote flowering in *Arabidopsis.* Plant Physiol. **139:** 770-778.

Yoo, S.K., Wu, X., Lee, J.S., and Ahn, J.H. (2011). AGAMOUS-LIKE 6 is a floral promoter that negatively regulates the FLC/MAF clade genes and positively regulates FT in *Arabidopsis*. Plant J. **65:** 62-76.

Yu, G., Wang, L.G., Han, Y., and He, Q.Y. (2012). clusterProfiler: An R package for comparing biological themes among gene clusters. OMICS **16:** 284-287.

Zaborowska, J., Egloff, S., and Murphy, S. (2016). The pol II CTD: New twists in the tail. Nat. Struct. Mol. Biol. **23:** 771-777.

Zhang, C., Du, X., Tang, K., Yang, Z., Pan, L., Zhu, P., Luo, J., Jiang, Y., Zhang, H., Wan, H., Wang, X., Wu, F., Tao, W.A., He, X.J., Zhang, H., Bressan, R.A., Du, J., and Zhu, J.K. (2018). *Arabidopsis* AGDP1 links H3K9me2 to DNA methylation in heterochromatin. Nat. Commun. **9:** 4547.

Zhang, X., Clarenz, O., Cokus, S., Bernatavichute, Y.V., Pellegrini, M., Goodrich, J., and Jacobsen, S.E. (2007a). Whole-genome analysis of histone H3 lysine 27 trimethylation in *Arabidopsis*. PLoS Biol. **5:** e129.

Zhang, X., Germann, S., Blus, B.J., Khorasanizadeh, S., Gaudin, V., and Jacobsen, S.E. (2007b). The *Arabidopsis* LHP1 protein colocalizes with histone H3 Lys27 trimethylation. Nat. Struct. Mol. Biol. **14:** 869-871.

Zhang, Y.Z., Yuan, J., Zhang, L., Chen, C., Wang, Y., Zhang, G., Peng, L., Xie, S.S., Jiang, J., Zhu, J.K., Du, J., and Duan, C.G. (2020). Coupling of H3K27me3 recognition with transcriptional repression through the BAH-PHD-CPL2 complex in *Arabidopsis*. Nat. Commun. **11:** 6212.

Zhao, D., Zhang, X., Guan, H., Xiong, X., Shi, X., Deng, H., and Li, H. (2016). The BAH domain of BAHD1 is a histone H3K27me3 reader. Protein Cell **7:** 222-226.

Zhao, Q.Y., and He, X.J. (2018). Exploring potential roles for the interaction of MOM1 with SUMO and the SUMO E3 ligase-like protein PIAL2 in transcriptional silencing. PLoS One **13:** e0202137.

Zhao, S., Zhang, B., Yang, M., Zhu, J., and Li, H. (2018). Systematic profiling of histone readers in *Arabidopsis thaliana*. Cell Rep. **22:** 1090-1102.

Zhou, J.X., Liu, Z.W., Li, Y.Q., Li, L., Wang, B., Chen, S., and He, X.J. (2018). *Arabidopsis* PWWP domain proteins mediate H3K27 trimethylation on FLC and regulate flowering time. J. Integr. Plant Biol. **60:** 362-368.

Zhou, Y., Romero-Campero, F.J., Gomez-Zambrano, A., Turck, F., and Calonje, M. (2017). H2A monoubiquitination in *Arabidopsis thaliana* is generally independent of LHP1 and PRC2 activity. Genome Biol. **18:** 69.

FIGURE LEGENDS

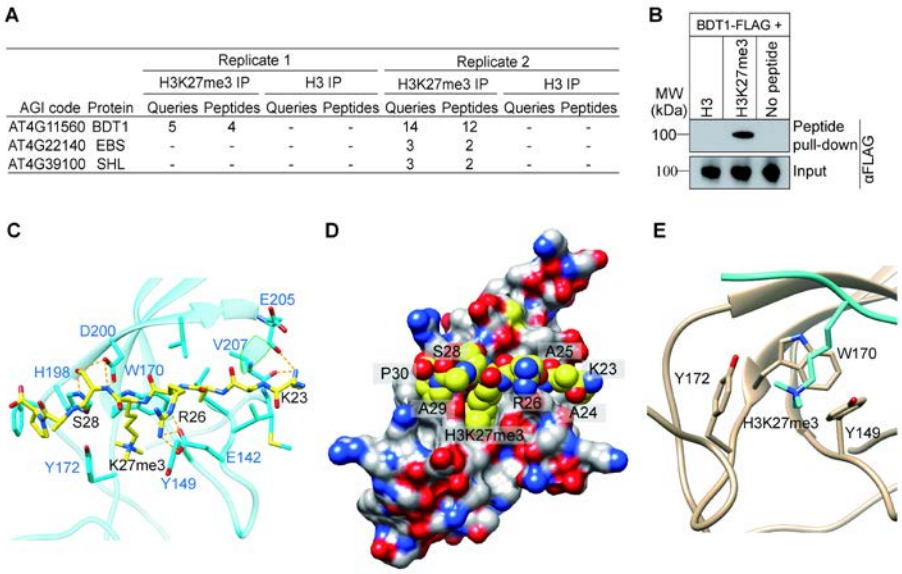

Figure 1. Identification of BDT1 as a reader of tri-methylated H3K27 peptide

(**A**) Identification of proteins by IP-MS from peptide affinity purification using H3K27me3 peptide or unmodified H3 peptide. (**B**) BDT1 is co-purified with H3K27me3 peptide but not unmodified H3 peptide as determined by peptide affinity purification followed by immunoblotting using anti-FLAG antibody. (**C**) Details of specific recognition of tri-methylated H3K27 by an aromatic cage of BAH. The hydrogen-bonding interactions are indicated with dashed lines. (**D**) An electrostatic surface view of the modeled BDT1-BAH domain with H3K27me3 peptide. (**E**) An enlarged view of the BAH aromatic cage accommodating H3K27me3.

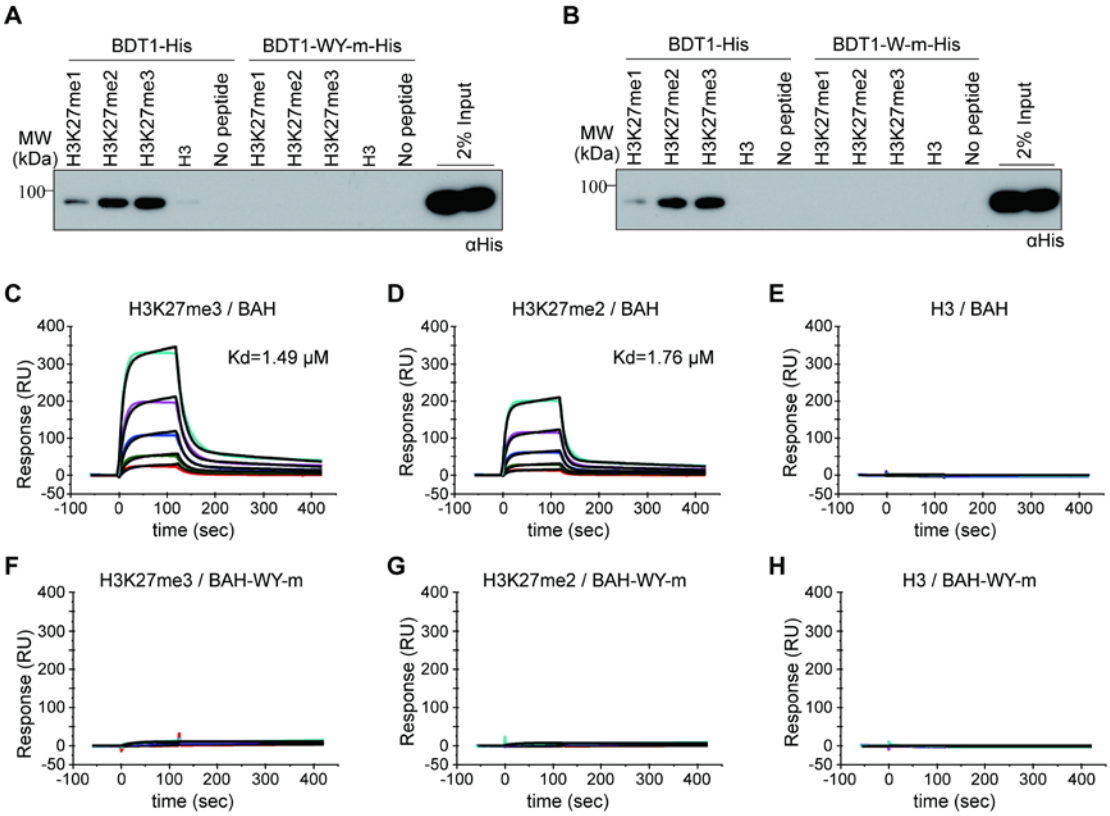

Figure 2. Binding of BDT1 to H3 peptides with mono-, di-, and tri-methylated H3K27 and unmodified H3 peptides

(**A** and **B**) The specific binding of BDT1-His but not BDT1-WY-m-His (**A**) or BDT1-W-m-His (**B**) to tri- and di-methylated H3K27 peptides, as determined by peptide pull-down followed by immunoblotting using anti-His antibody. (**C**-**E**) BIAcore assays of BDT1-BAH-GST protein bound to H3K27me3 (**C**), H3K27me2 (**D**), and H3 (**E**) peptides. The concentrations of loaded proteins are 2,000 (aqua), 1,000 (pink), 500 (blue), 250 (dark green), and 125 (red) nM. The fitting curves (black) and Kd values are denoted when they are available. (**F**-**H**) BIAcore assays of BDT1-BAH-WY-m-GST protein bound to H3K27me3 (**F**), H3K27me2 (**G**), and H3 (**H**) peptides. The concentrations of loaded proteins are the same as described in (**C**-**E**).

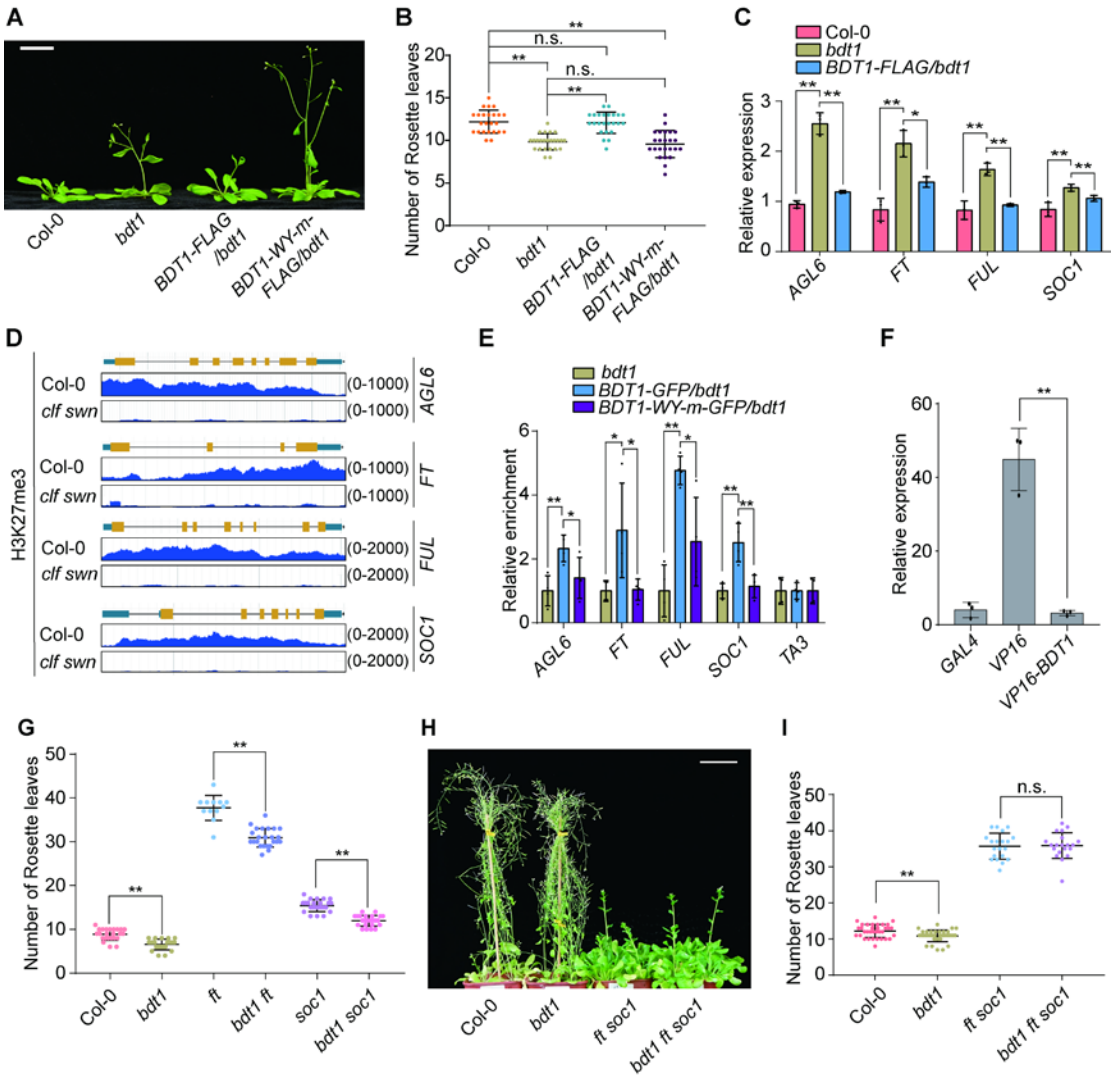

Figure 3. BDT1 is associated with and represses the transcription of flowering genes

(**A**) Morphological phenotypes of the WT Col-0 and of the *bdt1* and *bdt1* mutants transformed with WT *BDT1-FLAG* or site-mutated *BDT1-WY-m-FLAG*. Plants were photographed when 25 days old. Bar = 3 cm. (**B**) Numbers of rosette leaves in the indicated genotypes described. Black horizontal lines represent the means, and the error bars represent ± S.D. (**C**) Relative mRNA levels of selected flowering genes in the indicated genotypes. Values are means ± S.D. of three

biological repeats. Asterisks indicate significant differences between the two indicated samples, as determined by Student's *t*-test (** $P<0.01$, * $P<0.05$). (**D**) Genome-browser view of normalized H3K27me3 deposition at indicated loci. Diagrams of genes are shown in the top panel. Blue boxes, yellow boxes, and lines represent untranslated regions, coding regions, and introns, respectively. (**E**) ChIP-qPCR showing the relative enrichment of BDT1-GFP and BDT1-WY-m-GFP in selected flowering genes loci. Values are means ± S.D. of four technical repeats from two biological repeats. Asterisks indicate significant differences between the two indicated samples, as determined by Student's *t*-test (** $P<0.01$, * $P<0.05$). (**F**) Transcriptional repression ability of BDT1 as determined by a luciferase reporter assay. The *BDT1* gene was fused with *GAL4-BD-VP16* and was then expressed for the reporter assay. (**G**) Numbers of rosette leaves of Col-0, *bdt1*, *ft soc1*, *bdt1 ft*, and *bdt1 soc1*. Black horizontal lines represent the mean, and the error bars represent ± S.D. (**H**). Morphological phenotypes of the WT Col-0 and of the *bdt1*, *ft soc1*, and *bdt1 ft soc1* mutants. Plants were photographed when 58 days old. Bar=5 cm. (**I**) Numbers of rosette leaves in the genotypes described in H. Black horizontal lines represent the mean, and the error bars represent ± S.D. In (**B**), (**G**), and (**I**), number of rosette leaves were determined for at least 20 plants of each genotype; asterisks indicate significant differences between the two indicated genotypes, as determined by Student's *t*-test (** $P<0.01$).

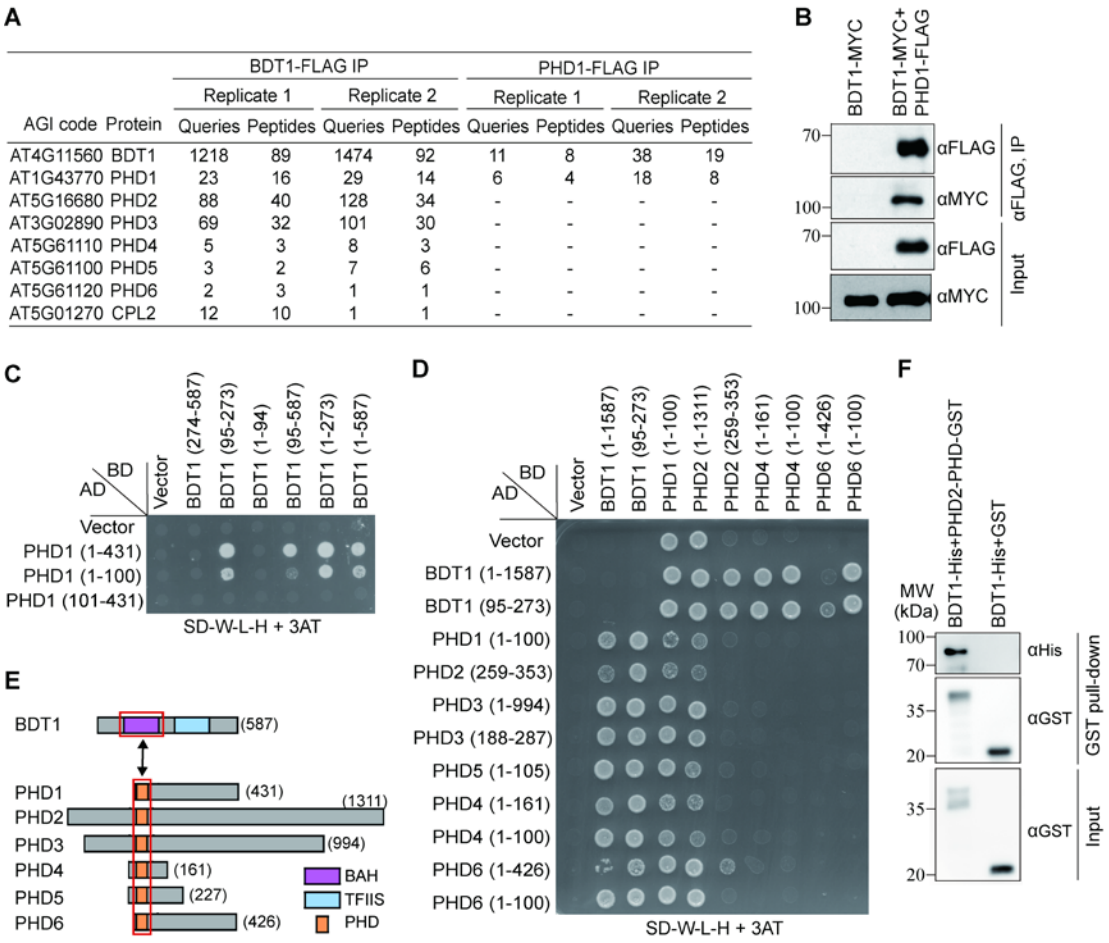

Figure 4. Interaction of BDT1 with a family of PHD finger-containing proteins and CPL2

(**A**) Identification of proteins by IP-MS from *BDT1-FLAG* and *PHD1-FLAG* transgenic plants. (**B**) Interaction between BDT1 and PHD1 as determined by co-IP.

(**C**) Identification of the domains required for BDT1-PHD1 interaction as determined by Y2H assays. (**D**) Interactions between the BAH domain of BDT1 and the PHD domains of PHD proteins as determined by Y2H assays. (**E**)

Diagram showing the domains responsible for the interaction between BDT1 and PHD proteins. (**F**) The interactions between BDT1-His and PHD2-PHD-GST as determined by GST pull-down assay.

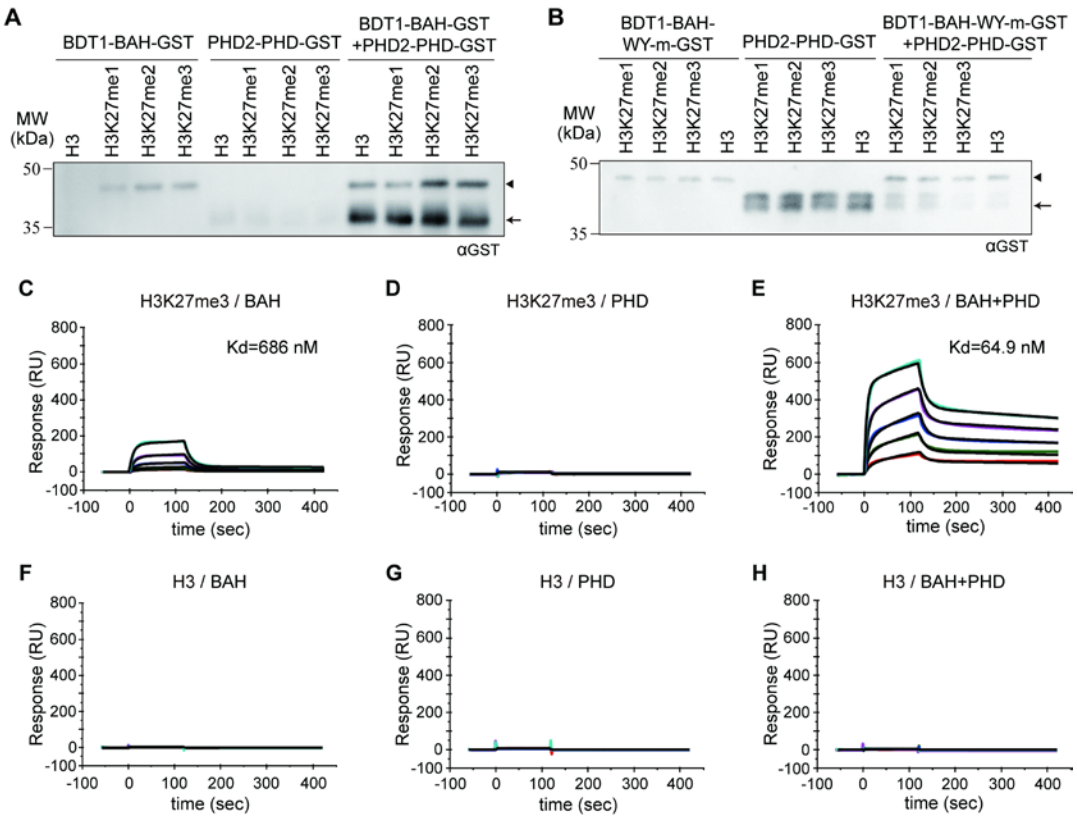

Figure 5. The BAH-PHD module has a higher binding affinity to H3K27me3 than either BAH or PHD

(**A**) Addition of PHD2-PHD-GST increased the binding affinity of BDT1-BAH-GST to H3K27me3 as determined by peptide pull-down followed by immunoblotting using anti-GST antibody. The arrow head and arrow indicate BDT1-BAH-GST and PHD2-PHD-GST, respectively. (**B**) Addition of

PHD2-PHD-GST had no effect on the binding ability of BDT1-BAH-WY-m-GST to H3K27me3 as determined by peptide pull-down followed by immunoblotting using anti-GST antibody. The arrow head and arrow indicate BDT1-BAH-WY-m-GST and PHD2-PHD-GST, respectively. (C-H) BIAcore diagrams showing the interaction of BDT1-BAH-GST protein (**C**, **F**), PHD2-PHD-GST protein (**D**, **G**), and pre-incubated BDT1-BAH-GST protein with PHD2-PHD-GST protein (**E**, **H**) with H3K27me3 (**C**-**E**) and H3 peptides (**F**-**H**). Concentrations of the flow-through proteins are 2,000 (aqua), 1,000 (pink), 500 (blue), 250 (dark green), and 125 (red) nM. The fitting curves (black) and Kd values are denoted when they are available.

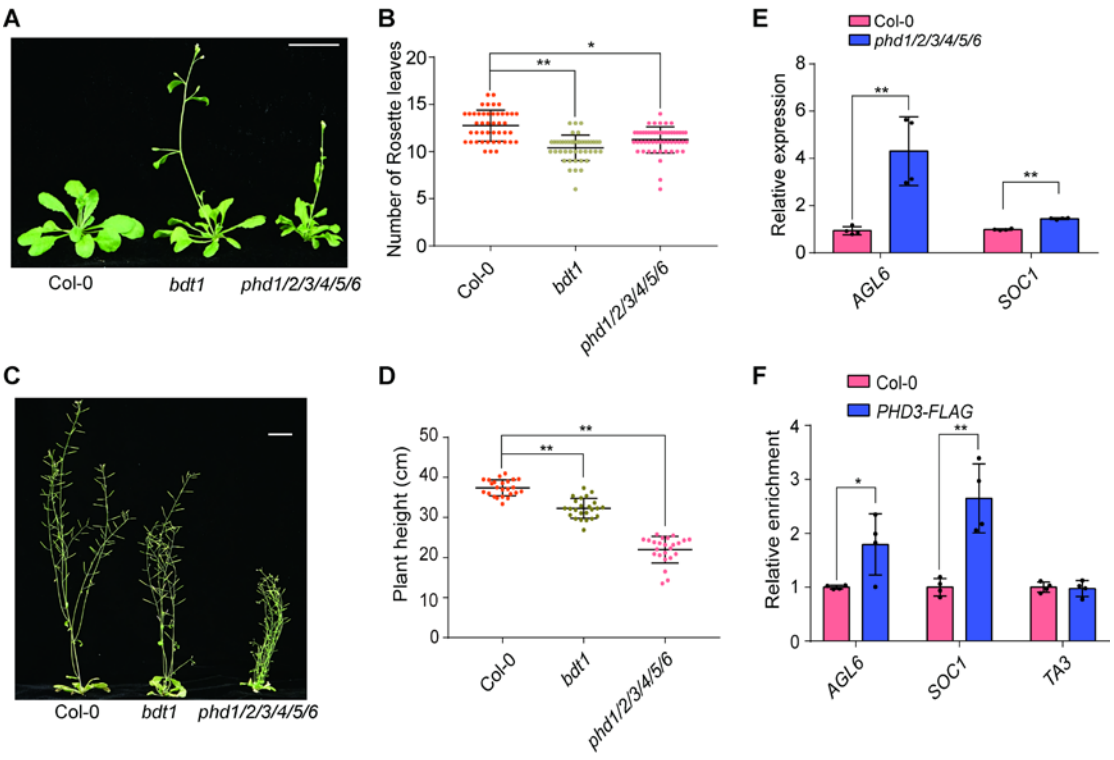

Figure 6. The *phd1/2/3/4/5/6* sextuple mutant shows early flowering and pleiotropic developmental defects

(**A**) Morphological phenotypes of 25-day-old plants of Col-0, *bdt1*, and *phd1*/*2*/*3*/*4*/*5*/*6*. Bar = 3 cm. (**B**) Numbers of rosette leaves in the indicated genotypes. Black horizontal lines represent the mean, and the error bars represent ± S.D. At least 20 plants for each genotype were included for the analysis. Asterisks indicate significant differences between the two indicated genotypes, as determined by Student's *t*-test (** $P<0.01$, * $P<0.05$). (**C**) Morphological phenotypes of 40-day-old plants of the indicated genotypes. Bar = 3 cm. (**D**) Height of adult plants of the indicated genotypes. Black horizontal lines represent the mean, and the error bars represent ± S.D. At least 20 plants for each genotype were included for the analysis. Asterisks indicate significant differences between the two indicated genotypes, as determined by Student's *t*-test (** $P<0.01$). (**E**) Relative mRNA levels of selected flowering genes in the indicated genotypes. Values are means ± S.D. of four technical repeats from two biological repeats. Asterisks indicate significant differences between the two indicated samples, as determined by Student's *t*-test (** $P<0.01$). (**F**) ChIP-qPCR showing the relative enrichment of PHD3-FLAG in selected flowering genes. Values are means ± S.D. of four technical repeats from two biological repeats. Asterisks indicate significant differences between the two indicated samples, as determined by Student's *t*-test (** $P<0.01$, * $P<0.05$).